ACS APPLIED MATERIALS & INTERFACES

www.acsami.org

Research Article

Role of Exciton Lifetime, Energetic Offsets, and Disorder in Voltage Loss of Bulk Heterojunction Organic Solar Cells

Rakesh Suthar, Abhijith T, Hemraj Dahiya, Abhishek Kumar Singh, Ganesh D Sharma, and Supravat Karak*

Cite This: https://doi.org/10.1021/acsami.2c18199

Read Online

ACCESS | Metrics & More | Article Recommendations | Supporting Information

ABSTRACT: Recently, the power conversion efficiency (PCE) of organic solar cells (OSCs) has significantly progressed with a rapid increase from 10 to 19% due to state-of-the-art research on nonfullerene acceptor molecules and various device processing strategies. However, OSCs still exhibit significant open circuit voltage loss ($\Delta V_{OC} \sim 0.6$ V) due to high energetic offsets and molecular disorder. In this work, we present a systematic investigation to determine the effects of energetic offset and disorder on different recombination losses in open circuit voltage (V_{OC}) using 13 different photoactive layers, wherein the PCE and ΔV_{OC} vary in the ranges of 2.21−14.74% and 0.561−1.443 V, respectively. The detailed voltage loss analysis of all these devices was carried out, and voltage losses were correlated with energetic offset and disorder. This has enabled us to identify the key features for minimizing the voltage loss like: (1) a low energy offset between the donor and acceptor molecular states is essential to attain a nonradiative voltage loss ($\Delta V_{OC, nrad}$) as low as ∼200 meV and (2) Urbach energy, which is a measure of the materials' disorder and packing, should be low for the minimization of the radiative voltage loss ($\Delta V_{OC, rad}$). In addition, time-resolved photoluminescence spectroscopy was employed to further understand the exciton dynamics of pristine materials and donor−acceptor blends. It was observed that the absorbers with ultralong exciton lifetime (∼1000 ps) produce higher efficiencies. The current study emphasizes the importance of simultaneously testing photovoltaic performance and active layer exciton dynamics for rational device optimization and opens new prospects for designing novel molecules with fine-tuning of energetic offset and disorder with longer exciton lifetime which is the effective strategy to boost the efficiency of OSCs to their modified Shockley−Queisser (SQ) limit by minimizing radiative and nonradiative voltage losses.

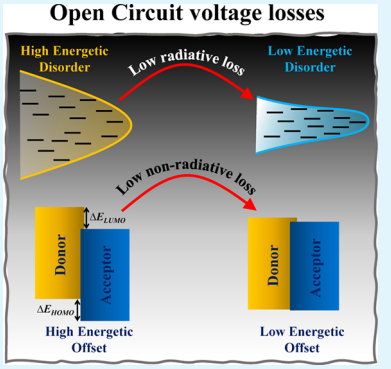

KEYWORDS: *organic solar cell, voltage loss, energetic offset, Urbach energy, exciton lifetime*

INTRODUCTION

Over the last few years, organic solar cells (OSCs) have emerged as one of the promising third generation photovoltaic technologies due to the unprecedented improvement in their device performance.[1−4] Owing to its unique advantages like low production cost, roll-to-roll solution processability, lightweight, and mechanical flexibility, this technology has potential in the eco-friendly photovoltaic market, especially in building integrated photovoltaics.[1,2,5−7] A certain threshold in power conversion efficiency (PCE), device stability, and production cost needs to be achieved for future commercialization of OSCs.[8−11] At present, the PCE has been improved more than 19% in single-junction solar cells,[12−18] which is largely driven by the state-of-the-art research in developing nonfullerene acceptor (NFA) materials, device optimization, and understanding the working mechanism.[3,19,20] Although a high PCE has been often reported, their open circuit voltage (V_{OC}) lags behind that of inorganic counterparts, indicating that V_{OC} loss (ΔV_{OC}) in OSCs is still substantial.[21−25] The charge transfer (CT) state at the donor−acceptor interface and the different recombination processes of charge carriers are the main contributing factors to ΔV_{OC}.[26−28] Until recently, it was recognized that the energy level offset between the highest occupied molecular orbital (HOMO) and lowest unoccupied molecular orbital (LUMO) of at least 0.3 eV is necessary to obtain a fast and efficient charge generation at the donor−acceptor (D/A) interface.[29−32] This energy level offset generally limits the further improvement in the performance of fullerene-based OSCs.[1,3] However, with a rapid development in NFAs and conjugate polymers, previous studies have shown that efficient free charge generation can be maintained even at a lower HOMO energy offset (ΔE_{HOMO}) below 0.2 eV.[3,19,26,33−35] Many studies on voltage loss based on the Shockley−Queisser (SQ) theory have demonstrated that the V_{OC} loss in NFA-based devices can be reduced near to 0.4 V

Received: October 10, 2022
Accepted: December 28, 2022

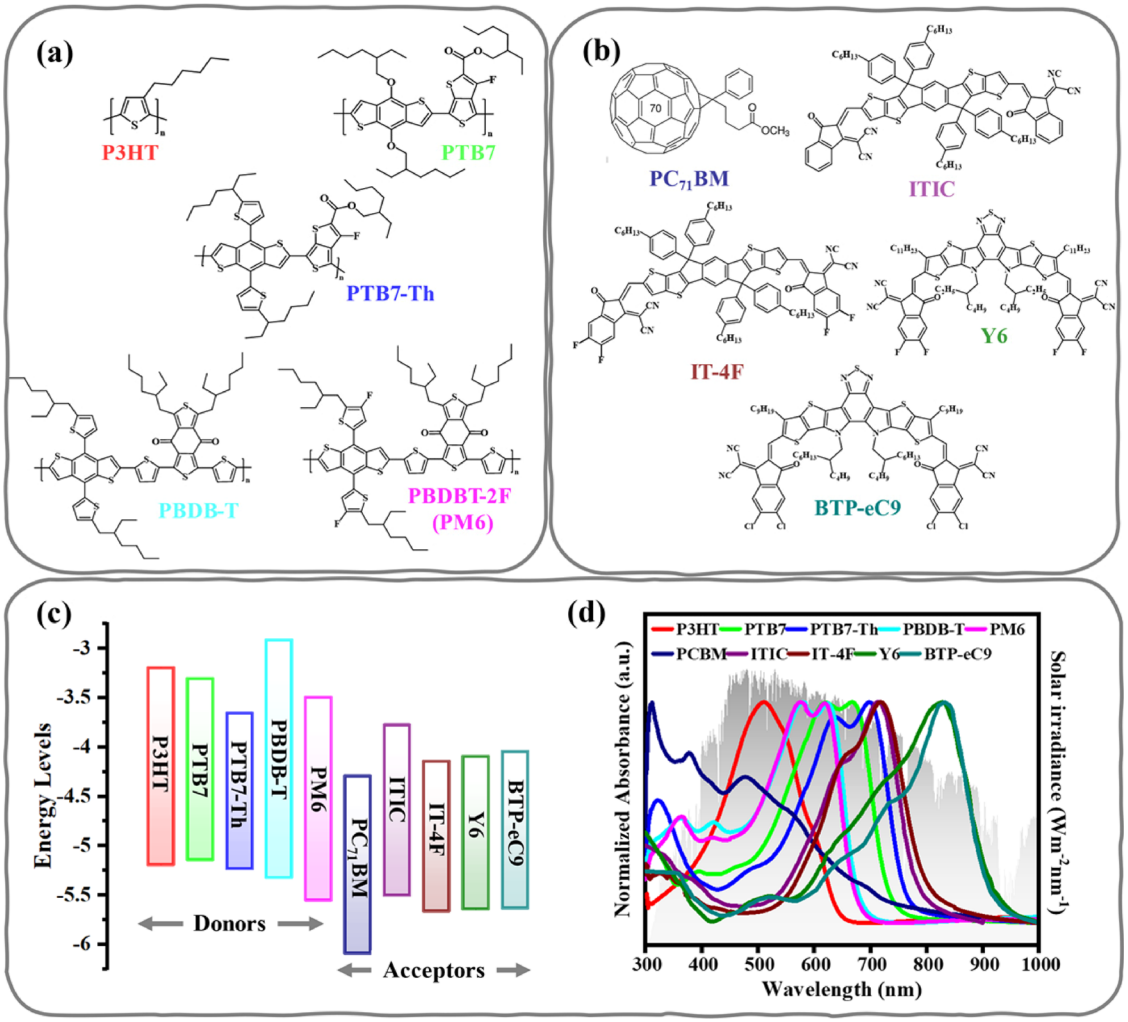

Figure 1. Materials, energy levels, and absorption spectra. (a, b) Chemical structures of the polymer donors (P3HT, PTB7, PTB7-Th, PBDB-T, and PM6) and acceptors (PCBM, ITIC, IT-4F, Y6, and PTB-eC9) investigated in the present study, (c) HOMO and LUMO energy levels of materials, and (d) normalized UV−vis absorption spectra of the materials in thin film and for a comparison, the photon flux of the AM 1.5G solar spectrum is shown on the right axis.

without losing the high external quantum efficiency (EQE) if the energy level offset decreases below 0.2 eV.[14,21,34,36,37] In addition to energetic offsets, earlier reports have revealed that the nature and degree of energetic disorder in the band edge of photoactive layer absorption and the exciton lifetime are also highly correlated with the charge carrier recombination.[38−43]

In recent years, several researchers have investigated the effects of energetic offsets, energetic disorder, and exciton lifetime on the total voltage loss in OSCs.[26,28,35,42,44,45] For instance, Qian et al. formulated a design rule for the minimization of total voltage loss by combining the spectroscopic and quantum chemistry approaches.[37] Their findings showed that the low energy offset and high photoluminescence (PL) yield of low bandgap materials in the active layer are essential to reduce the total voltage loss. Similarly, Hou and co-workers have systematically studied the effects of energy level offsets on exciton dissociation efficiency and total voltage loss.[46] This work suggested that a high PCE is attainable in nonfullerene-based devices as ΔE_{HOMO} approaches a threshold value. Below this particular value, the probability of exciton dissociation drastically reduces without affecting the charge transport process. In a different approach, Cao and co-workers investigated the influence of energetic disorder on the performance of OSCs.[47] Compared to fullerene-based devices, the NFA devices exhibited a low energetic disorder due to the torsion free molecular conformation of acceptor materials, leading to an improvement in charge transport and total voltage loss. Recently, Classen et al. explored the role of exciton lifetime in the charge generation in different D/A systems with low energetic offsets.[42] It was observed that in some photoactive layers with small ΔE_{HOMO}, the ultralong exciton splitting lifetime higher than the exciton lifetime of pristine material limits the performance of devices. Based on the theoretical analysis, Xie et al. suggested the upper thermodynamic limit of PCE (~31%) in single-junction OSCs using the radiative efficiency measurements, which was found to be slightly below the SQ limit and showed substantial room for improvement in the performance of OSCs.[35] Although there have been extensive studies on the effect of energetic offset, energetic disorder, and exciton lifetime on the total voltage losses in OSCs, a systematic investigation that demonstrates the correlation of energetic offset with the nonradiative voltage loss and energetic disorder with the radiative voltage loss in fullerene- and NFA-based devices remains unexplored in order to achieve the radiative efficiency limit.

https://doi.org/10.1021/acsami.2c18199
ACS Appl. Mater. Interfaces XXXX, XXX, XXX−XXX

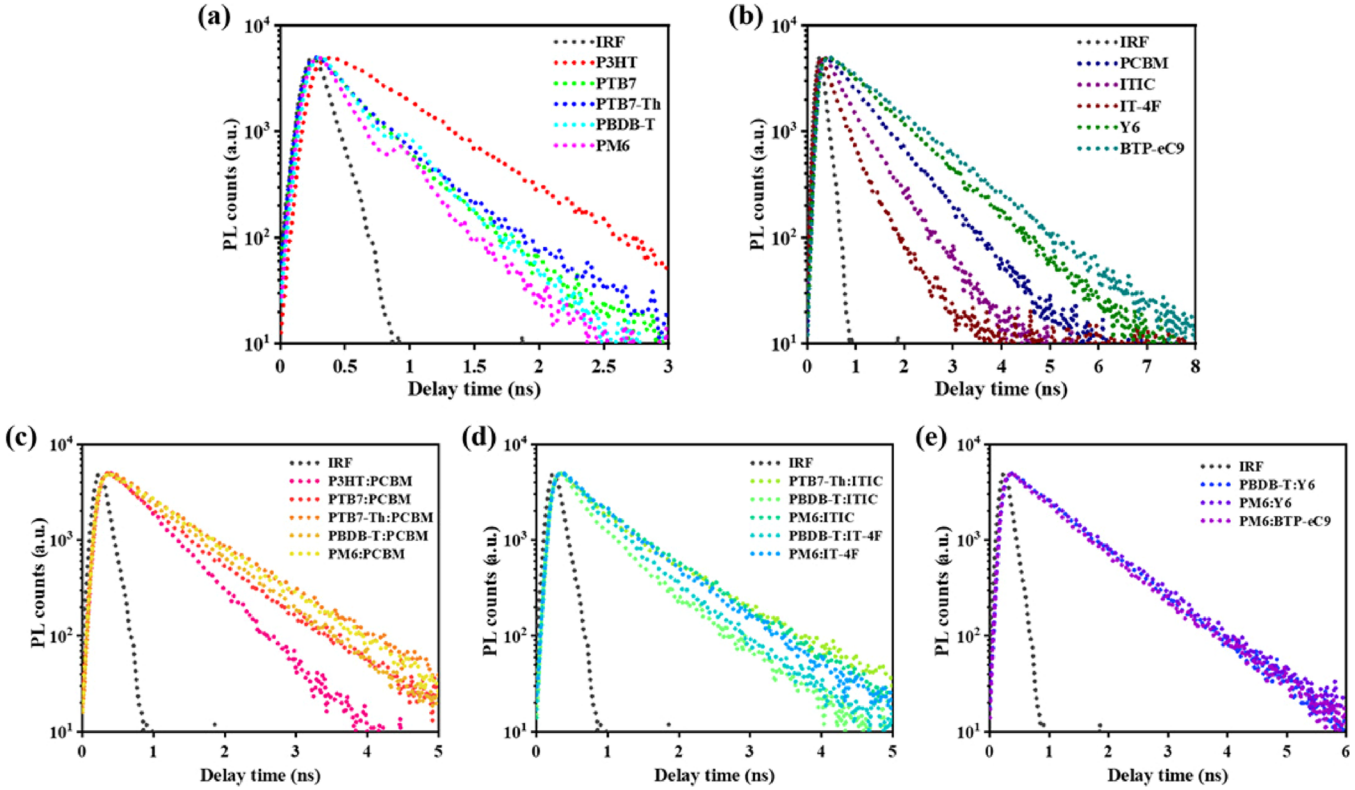

Figure 2. Exciton dynamic of the pristine donor, acceptor, and used photoactive layer (a, b) TRPL decay profiles of pristine donor and acceptor materials. (c−e) TRPL of all the photoactive layers investigated in the present study.

In this study, we examined the relationship of molecular energetic disorder and offsets with the different recombination losses using a series of different conjugated polymer donors in conjunction with fullerene and NFAs. For this purpose, we comprehensively measure the time-resolved photoluminescence (TRPL) decay profiles to assess the exciton dynamics particularly the exciton lifetime of pristine materials and the PL quenching lifetime of the photoactive layer. The OSCs were fabricated with 13 different photoactive layers, and current−voltage characteristics and EQE spectra were recorded for the voltage loss analysis via a detailed balance approach. It was observed that reducing the energetic offset leads to a reduction in the nonradiative recombination loss; on the other hand, reducing the energetic disorder decreases the radiative recombination loss. These findings suggest that the prolonged exciton lifetime of acceptor materials is essential to attain an efficient charge separation in the limit of small driving force, at well-matched energy levels and lower energetic disorder. In our view, this study will provide a valuable platform for researchers to get more insights into exciton dynamics and different voltage losses for the development of highly efficient OSCs.

RESULTS AND DISCUSSION

Donor−Acceptor Systems with Different Energy Offsets. To study the constraints in the device operation of OSCs, we investigated a series of donor (P3HT, PTB7, PTB7-Th, PBDB-T, and PM6) and acceptor (PCBM, NFAs like ITIC, IT-4F, Y6, and BTP-eC9) combinations. Figure 1a,b shows the chemical structures of donors and acceptors used in the present study. A full overview of the molecular energy levels of these materials based on previous reports is presented in Figure 1c and Table S2, which allows us to choose various molecular combinations with systematic variation of HOMO-HOMO offset (ΔE_{HOMO}) and LUMO-LUMO offset (ΔE_{LUMO}) offset in a wide range of −0.05 to 0.95 eV and 0.12−1.1 eV, respectively for the current study. The corresponding UV−vis absorption spectra of spin-coated films of each donor and acceptor are shown in Figure 1d. The standard AM 1.5G spectra are also included in the background which confirm the broad range spectral overlapping of active layer materials with input solar irradiance.

Exciton Dynamics of D−A Systems. The exciton dynamics of materials such as exciton lifetime of pristine donors and acceptors, and PL quenching lifetime of D/A blend plays important roles in the device performance.[42,43,48,49] In this work, TRPL spectroscopy was employed to investigate the potential correlation of exciton dynamics in the pristine donor and acceptor materials, and their different active layer systems with the devices performance are shown in Figure 2. Figure 2a,b displays the TRPL decay profiles for each pristine donor film and acceptor film measured at a wavelength, where the materials exhibit the maximum PL intensity. The singlet exciton lifetime of the pristine donor materials was found to be low around the ∼300 ps except P3HT (575 ps) (Figure 2a). On the other hand, pristine acceptor materials exhibited a substantial spread in singlet exciton lifetime from picosecond to few nanoseconds. The fullerene acceptor showed an exciton lifetime of around 689 ps, which is consistent with the previous reports.[49] Interestingly, the novel A-DA′D-A NFAs, Y6, and BTP-eC9 exhibited the longest exciton lifetime of 1.03 and 1.11 ns, respectively. On the other hand, in the case of D/A blends, the experimentally obtained exciton decay rate represents the PL quenching lifetime, which is not a direct measure of the exciton lifetime or the lifetime of exciton

https://doi.org/10.1021/acsami.2c18199
ACS Appl. Mater. Interfaces XXXX, XXX, XXX−XXX

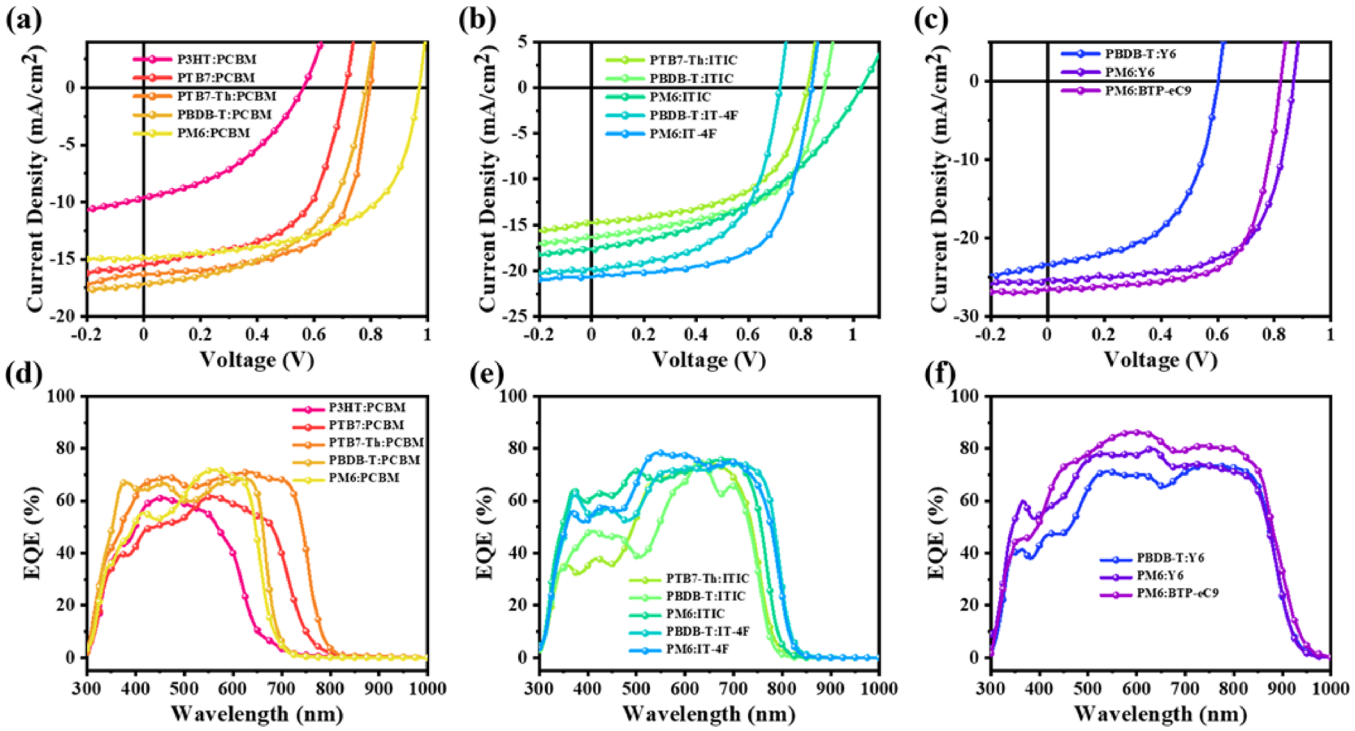

Figure 3. Photovoltaic characterization of three different groups of devices (a–c) *J*–*V* characteristics of all the best performing OSCs under AM 1.5G illumination at 1 SUN, and (d–f) external quantum efficiency of corresponding devices.

Table 1. Photovoltaic Performance Parameters for the Fabricated OSCs Extracted from *J*–*V* Characteristics under AM 1.5G Illumination

sr. no.	donor	acceptor	ΔE_{HOMO} (eV)	ΔE_{LUMO} (eV)	J_{SC} (mA/cm^2)	integrated J_{SC} (mA/cm^2)	V_{OC}(V)	FF (%)	PCE (%)	Avg PCE (%)
group 1	P3HT	PCBM	0.9	1.1	9.60	8.90	0.560	41.10	2.21	1.95 ± 0.21
	PTB7	PCBM	0.95	0.99	15.88	15.21	0.720	55.92	6.40	6.24 ± 0.29
	PTB7-Th	PCBM	0.86	0.64	16.29	15.82	0.800	63.22	8.24	8.02 ± 0.30
	PBDB-T	PCBM	0.77	1.38	16.86	16.36	0.840	55.35	7.84	7.42 ± 0.27
	PM6	PCBM	0.54	0.8	14.84	13.95	0.964	59.25	8.47	8.20 ± 0.32
group 2	PTB7-Th	ITIC	0.27	0.12	14.78	14.19	0.820	55.67	6.75	6.52 ± 0.21
	PBDB-T	ITIC	0.18	0.86	16.36	15.37	0.880	55.46	7.99	7.62 ± 0.35
	PM6	ITIC	−0.05	0.28	17.68	17.40	1.024	42.79	7.75	7.47 ± 0.29
	PBDB-T	IT-4F	0.34	1.23	19.82	18.62	0.716	57.02	8.10	7.92 ± 0.19
	PM6	IT-4F	0.11	0.65	20.42	19.53	0.800	63.43	10.36	10.18 ± 0.21
group 3	PBDB-T	Y6	0.32	1.18	23.33	22.80	0.600	54.56	7.64	7.50 ± 0.15
	PM6	Y6	0.09	0.6	25.22	24.64	0.860	66.00	14.32	14.05 ± 0.39
	PM6	BTP-eC9	0.08	0.55	26.47	25.93	0.820	67.90	14.74	14.49 ± 0.32

splitting individually. The decay of PL in the active layer is caused by both mechanisms, and hence the measured lifetime consists of both the components of exciton lifetime and lifetime of exciton splitting. The measured decay profiles of 13 different D/A blends are shown in Figure 2c–f, and the calculated lifetimes are summarized in Table S4. The PCBM-based blends exhibited the PL quenching lifetime in a range of 613–719 ps. Slightly lower PL quenching lifetime (383–689 ps) was observed in the case of ITIC-based blends, which impacted not only the efficiency of the exciton separation but also the kinetics of recombination processes via CT states. Compared to these blends, the Y-series-based blends showed a higher lifetime in a range of 804–958 ps, leading to a high exciton splitting efficiency and an increased exciton diffusion length that enhance the exciton dissociation.[43,49] The extracted PL decay lifetimes for all the pristine materials and D/A blends are listed in Table S4. A previous experimental study also showed a similar trend in results that a long singlet exciton lifetime of absorber is crucial for maintaining efficient charge generation at low ΔE_{HOMO}, which was further verified by an analytical model based on the Boltzmann stationary state equilibrium between the local exciton (LE) and the CT states.[42] Our key conclusion as a design rule for OSCs close to the radiative limit is that the prolonged exciton lifetime of acceptor materials is essential for an efficient charge generation process.

Photovoltaic Properties. To study the effects of energetic offsets and associated voltage loss, inverted OSCs using 13 different D/A blends with the device structure ITO/ZnO/active layer/MoO_3/Ag were fabricated. The device fabrication parameters for each active layer were taken from the literature, which are discussed in the Experimental Section. The

https://doi.org/10.1021/acsami.2c18199
ACS Appl. Mater. Interfaces XXXX, XXX, XXX–XXX

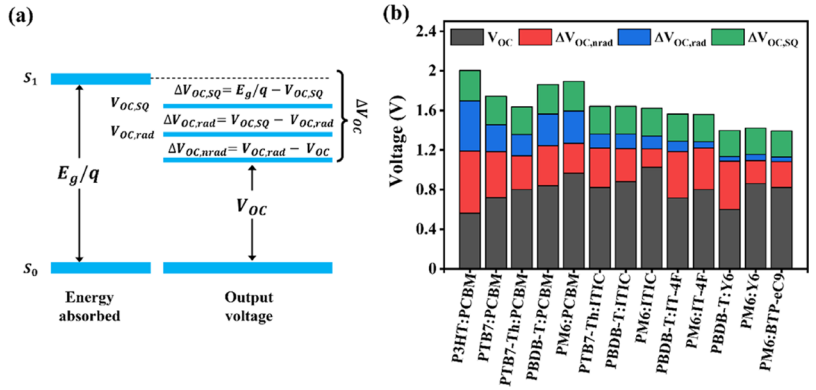

Figure 4. Voltage loss ananlysis (a) Schematic diagram for voltage losses of OSCs according to the detailed balanced theory, S_0, ground state; S_1, excited state (b) Bar plot of V_{OC} with three diffenrent parts of total voltage loss, ΔV_{SQ}, $\Delta V_{OC,rad}$, and $\Delta V_{OC,nrad}$.

Table 2. Voltage Loss Parameters by SQ Limits for Fullerene- and Nonfullerene Acceptor-Based Systems

sr. no.	donor	acceptor	E_g (eV)[a]	E_U (meV)	V_{OC} (V)	$V_{OC,SQ}$ (V)	$V_{OC,rad}$ (V)	ΔV_{SQ} (V)	$\Delta V_{OC,rad}$ (V)	$\Delta V_{OC,nrad}$ (V)	ΔV_{OC} (V)
group 1	P3HT	PCBM	2.003	105.4	0.560	1.697	1.190	0.306	0.507	0.630	1.443
	PTB7	PCBM	1.743	60.9	0.720	1.455	1.183	0.288	0.272	0.463	1.023
	PTB7-Th	PCBM	1.638	50.4	0.800	1.357	1.142	0.281	0.214	0.342	0.838
	PBDB-T	PCBM	1.861	58.9	0.840	1.565	1.242	0.296	0.323	0.402	1.021
	PM6	PCBM	1.892	45.9	0.964	1.594	1.266	0.298	0.328	0.302	0.928
group 2	PTB7-Th	ITIC	1.642	38.9	0.820	1.362	1.220	0.280	0.142	0.399	0.821
	PBDB-T	ITIC	1.641	28.71	0.880	1.361	1.214	0.280	0.146	0.334	0.761
	PM6	ITIC	1.621	27.0	1.024	1.342	1.211	0.279	0.131	0.187	0.597
	PBDB-T	IT-4F	1.564	33.0	0.716	1.289	1.184	0.275	0.104	0.468	0.848
	PM6	IT-4F	1.559	26.5	0.800	1.283	1.221	0.276	0.063	0.421	0.759
group 3	PBDB-T	Y6	1.397	28.6	0.600	1.133	1.087	0.264	0.046	0.487	0.797
	PM6	Y6	1.421	26.1	0.860	1.155	1.094	0.266	0.061	0.234	0.561
	PM6	BTP-eC9	1.392	24.2	0.820	1.129	1.083	0.263	0.045	0.263	0.572

[a]Bandgap (E_g) calculated for the first derivative of the EQE spectra.

photovoltaic performance parameters for all the photoactive layers are summarized in Table 2. To analyze the data systematically, these devices were divided into three different groups based on the acceptor generation. The devices fabricated by blending the PCBM acceptor with conjugate polymer donors were considered as group-1 (fullerene devices), which possesses ΔE_{HOMO} in a range of 0.5−0.95 eV and ΔE_{LUMO} in a range of 0.68−1.38 eV. The NFA devices based on ITIC series and novel A-DA′D-A Y-series as acceptors were considered in group-2 and group-3, respectively. The ΔE_{HOMO} values for some of the D−A blends in group 3 are very low around 0.08 eV.

Current density−voltage (J−V) characteristics and EQE spectra for each group are shown in Figure 3, and performance parameters are summarized in Table 1. The group-1 devices exhibited a high J_{SC} around ∼16 mA/cm^2 due to their high energy offsets that provide enough driving force for efficient charge generation.[31] The differences in J_{SC} values were mainly caused by the different absorption profiles of the conjugated polymers (Figure 1d). However, it should be noted that due to the large energetic offsets and hence high energy losses, the performance of devices is ultimately limited.[47] Therefore, we investigated the group-2 active layers with small ΔE_{HOMO}, which is beneficial to achieve a high J_{SC} and V_{OC} in the group 2 devices. The PM6:ITIC-based devices exhibited a higher V_{OC} of 1.024 V, due to its lower energetic offsets, ΔE_{HOMO} = −0.05 eV, and ΔE_{LUMO} = 0.28 eV. Nevertheless, the performance of group-2 devices is still limited due to poor molecular packing and lower singlet exciton lifetime. The superior performance of group-3 devices with high J_{SC} (∼25 mA/cm^2) and PCE around ∼15% at low ΔE_{HOMO} is mainly due to prolonged exciton lifetime and excellent light harvesting ability at higher wavelengths. These results revealed that the better performance of NFA-based OSCs than that of fullerene-based devices was attributed to their high J_{SC}. However, recently it was shown that the higher performance of the NFA-based OSCs is also due to low energetic offsets and improved molecular disorder in the D−A system. In this context, a detailed voltage loss analysis was carried out, and its correlation with the energetic offsets and disorder was systemically studied to identify the possible reasons for the different performance.

Voltage Loss Analysis. The voltage loss of each device contains the relevant information when different photoactive layers are compared, as these different D−A combinations exhibit unique bandgaps. Determining the accurate E_g value of photoactive layers is critical to precisely quantify the voltage loss in OSCs.[50,51] In the literature, several procedures were applied to determine the bandgaps of solar cells, However, only one method is based on a proper mathematical model, and it utilizes the device bandgap instead of a material bandgap.[52,53] In this work, the band edge of EQE spectra for different D/A blends was used for E_g calculation as shown in Figure S1. By utilizing this bandgap, the voltage loss of solar cells was investigated according to the SQ theory, which is expressed as $\Delta V_{OC} = E_g/q - V_{OC}$.[54] Furthermore, when comparing V_{OC} with its radiative and SQ limits, it allows us

https://doi.org/10.1021/acsami.2c18199
ACS Appl. Mater. Interfaces XXXX, XXX, XXX−XXX

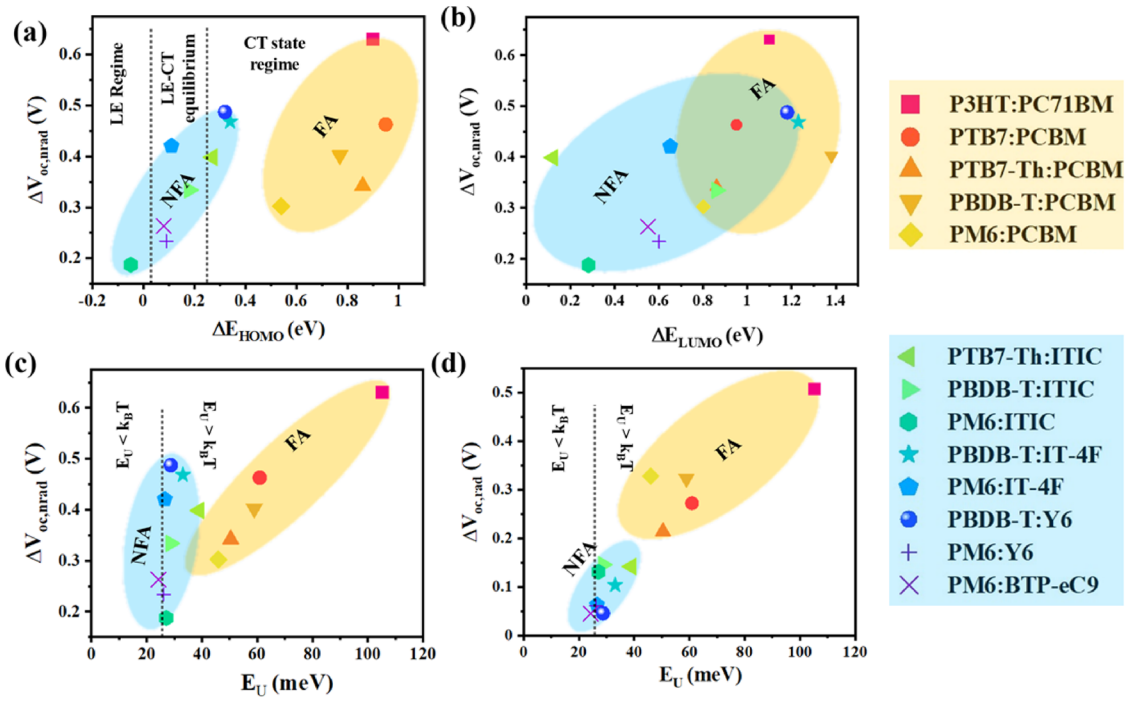

Figure 5. Correlation of the $\Delta V_{OC,\,nrad}$ and $\Delta V_{OC,\,rad}$ with the energetic offsets and Urbach energy (a, b) relationship of $\Delta V_{OC,\,nrad}$ v/s ΔE_{HOMO} and ΔE_{LUMO}, respectively, and (c, d) $\Delta V_{OC,\,nrad}$ and $\Delta V_{OC,\,rad}$ plotted with the Urbach energy.

to categorize the ΔV_{OC} into three different kinds of measurable or known losses, as shown in eq 3 (Experimental Section) and Figure 4a. The first term of the voltage loss ($\Delta V_{OC,\,SQ}$) represents the radiative recombination originating from the absorption above the bandgap, where $V_{OC,\,SQ}$ is the maximum voltage based on the SQ limit. The value of $\Delta V_{OC,\,SQ}$ depends on the bandgap of the photoactive layer, and it varies between 0.25 and 0.30 V, which is generally unavoidable for all kinds of photovoltaic technologies.[54] The second term in total voltage loss ($\Delta V_{OC,\,rad}$) is due to the additional radiative recombination within the bandgap, and the last term ($\Delta V_{OC,\,nrad}$) is the measure of nonradiative recombination loss. Due to the less emissive nature of organic semiconductors and the presence of CT states, ($\Delta V_{OC,\,nrad}$) in OSCs is quite higher than in inorganic or perovskite solar cells, being the critical barrier limiting the V_{OC} in OSCs.[23,52] Both $\Delta V_{OC,\,rad}$ and $\Delta V_{OC,\,nrad}$ can be reduced by better molecular level alignment and molecular packing of photoactive materials.[47]

The different voltage losses of all the fabricated devices are summarized in Table 2, and their comparison is shown in the bar graph (Figure 4b). The group 1 devices exhibited high ΔV_{OC} of 0.8−1.5 V owing to very strong nonradiative recombination, due to extremely low electroluminescence of the PCBM acceptor and sufficiently high energy offset at the D/A interface.[35] The group 2 devices possessed the well-aligned energetic offsets resulting in moderate ΔV_{OC} of 0.6−0.8 V. On the other hand, group 3 devices exhibited exceptionally low voltage losses (ΔV_{OC} ~ 0.5−0.6 V) with high J_{SC} resulting in an excellent performance. These devices showed very low $\Delta V_{OC,\,rad}$ (~0.05 V) and $\Delta V_{OC,\,nrad}$ (~0.3 V). The PM6:Y6-based devices exhibited $\Delta V_{OC,\,nrad}$ of 0.234 V, which is still significantly larger than that of other competitive technologies like GaAs (0.04 V), perovskite (0.06 V), etc., and this value is approaching close to the silicon (0.12 V) devices.[25,55,56] These results confirm the validity of prolonging the exciton lifetime and thus the exciton diffusion length to improve the photovoltaic performance of OSCs. Recently, it has been reported that low $\Delta V_{OC,\,nrad}$ ~ 0.25 V at low energy offsets, due to the higher electrostatic surface potential difference between the donor and acceptor, results in hybridization of CT and LE states.[4,26] Similarly, the formation of the nonemissive triplet excitons is also responsible for the high energy loss in the OSCs.[57] Now we turn to investigate how each part of the voltage loss correlates with the energetic offsets and disorder of photoactive layers which limits the device performance.

Correlation of Energetic Offset with Nonradiative Voltage Loss. To get more information on the influences of energetic offsets on the nonradiative recombination loss at open circuit condition, $\Delta V_{OC,\,nrad}$ of the devices was plotted against ΔE_{HOMO} and ΔE_{LUMO} as shown in Figure 5a,b. A clear strong correlation was observed which indicated that the voltage loss due to nonradiative recombination decreases with decreasing ΔE_{HOMO} for both fullerene- and nonfullerene-based devices (Figure 5a). This observation shows that reducing the ΔE_{HOMO} close to zero is essential to reduce the nonradiative recombination process. The abrupt drop in $\Delta V_{OC,\,nrad}$ below 0.2 eV of ΔE_{HOMO} for NFA suggests the equilibrium between the LE state and CT state when excitonic state density is larger than the CT density.[26,42] However, the trend in the ΔE_{LUMO} v/s $\Delta V_{OC,\,nrad}$ plot is more scattered and irregularly distributed compared to the trend in the ΔE_{LUMO} v/s $\Delta V_{OC,\,nrad}$ plot, but it follows a similar pattern as the ΔE_{HOMO} was obeying. The results indicated that the nonradiative loss has little correlation with ΔE_{LUMO} because these values are relatively larger than ΔE_{HOMO}, and the driving force for exciton dissociation is mainly restricted by the distinct ΔE_{HOMO} values. The low value of $\Delta V_{OC,\,nrad}$ ~0.2 to 0.3 eV obtained in NFA-based devices with low offsets is the result of the electronic hybridization of the lowest LE state and CT state.[19,34,37]

Correlation of Energetic Disorder with Different Voltage Losses. For further understanding of voltage loss

https://doi.org/10.1021/acsami.2c18199
ACS Appl. Mater. Interfaces XXXX, XXX, XXX−XXX

relevant to overcome the current limitations concerning the development of NFA-based OSCs, we probed the electronic structure within the bandgap. The tail states are the main sources of energetic loss in OSCs, as charge carriers relax into these states and reduce the quasi-Fermi level splitting, leading to a reduction in V_{OC}.[58] The degree of energetic disorder was extracted from the exponentially shaped curve near band edge of EQE spectra in a higher wavelength region (where CT-assisted absorption not taken into account), which is referred as the Urbach energy (E_U). The detailed fitting procedure is discussed in the Experimental Section, and corresponding fitted curves are shown in Figure S2. The fullerene-based devices were affected by the high energetic disorder ($E_U \geq 40$ meV) due to a large degree of aggregation of the fullerene molecules in the photoactive layer.[9] On the other hand, the NFA-based devices showed very low energetic disorder, due to the presence of torsion free molecular backbone in NFAs.[41] To get more details of charge carrier recombination kinetics, both the voltage losses of the devices, $\Delta V_{OC,\,nrad}$ and $\Delta V_{OC,\,rad}$, were plotted against E_U as shown in Figure 5c,d. $\Delta V_{OC,\,nrad}$ of NFA-based devices showed a lesser correlation with E_U. On the other hand, $\Delta V_{OC,\,rad}$ exhibited a higher correlation with E_U, indicating the significant role of molecular packing and degree of energetic disorder in reducing the radiative recombination loss. For all the active layers, we observed a general trend (Figure 5d) that $\Delta V_{OC,rad}$ decreases with a decrease in E_U. The NFA-based devices possessed a lower E_U compared to the fullerene-based devices, and the underlying reason is the presence of coplanar and rigid backbone in nonfullerene electron acceptors resulting in a remarkably narrow distribution of electronic trap states.[58] For the novel Y-series NFA-based devices, E_U is approaching near room-temperature thermal energy ($k_BT \sim 25.8$ meV), which shows that this particular energy is sufficient for the charge carriers to escape from the traps in tail states. The PM6:BTP-eC9 photoactive layer-based device showed a low E_U of 24.8 meV with a low $\Delta V_{OC,rad}$ of around 0.045 V, indicating that this photoactive layer exhibits greatly suppressed charge trapping into the electronic intrabandgap tail states compared to other photoactive layers. These findings show that molecular packing and disorder of the photoactive layers play vital roles with a low bandgap acceptor, crystallinity of molecules, and low interfacial energy offset, for developing high-performance OSCs. These results are similar to the conventional high-performance inorganic solar cells such as Si, GaAs, perovskites, etc. in which very few tail states ($E_U < k_BT$) below the bandgap are generally observed.[59−63] It is evident that the radiative loss occurs due to the tail state absorption of the photoactive layer, which can be minimized with a proper combination of D−A systems. Our observation shows good agreement with the expected relationship of V_{OC} with E_U.[64,65] A recent study also suggested that reducing the molecular vibration can lead to reduction in radiative voltage losses.[66] Therefore, the fine-tuning of the molecular structure effectively regulates the molecular packing behavior, and it consequently plays an important role in reducing the energetic disorder and hence lower radiative recombination loss.

CONCLUSIONS

In this paper, a systematic investigation on the role of exciton dynamic, energetic offsets, and disorder in the performance of fullerene- and NFA-based OSCs was carried out. The exciton dynamics of pristine materials and D/A blends measured using TRPL spectroscopy shows that a prolonged exciton lifetime of absorbers is essential, which is attributed to high exciton splitting efficiency and an increase in the exciton diffusion length. Inverted OSCs were fabricated using 13 various photoactive layers with different material energetic offsets for quantitative assessment of the energetic offsets and disorder on the voltage losses. PCE and ΔV_{OC} of the fabricated devices were in the ranges of 2.21−14.74% and 0.561−1.443 V, respectively. The exceptionally low voltage losses ($\Delta V_{OC} \sim$ 0.5−0.6 V) with high-performance A-DA′D-A acceptor devices with suitable donors are due to low offset and better molecular packing. In addition, the $\Delta V_{OC,\,rad}$ and $\Delta V_{OC,\,nrad}$ were correlated with the energetic offset and Urbach energy, and it was found that the high radiative recombination losses are due to higher energetic disorder, and the nonradiative recombination losses are mainly limited by the high ΔE_{HOMO}. These findings indicate that energetic offset and disorder of the photoactive layer play a vital role in the operation of OSCs in addition to the exciton dynamics, because their magnitudes strongly influence the efficiency of photoinduced charge separation hence the performance.

EXPERIMENTAL SECTION

Materials and Characterization. In this study, the OSCs with an inverted device architecture ITO/ZnO/photoactive layer/MoO_3/Ag were fabricated. For this purpose, five donors (P3HT, PTB7, PTB7-Th, PBDB-T, and PBDBT-2F (PM6)) and five acceptors (PCBM, ITIC, IT-4F, Y6, and BTP-eC9) were purchased from 1-Materials Inc. Canada and used without any further purification. The ZnO solution was prepared by following the sol−gel method using zinc acetate dehydrate (Sigma-Aldrich) as the precursor. All other materials and solvents were of common commercial standard and used as received. Steady-state UV−vis absorption spectra were recorded using a Shimadzu 2450 spectrophotometer.

TRPL Measurement. TRPL spectroscopy measurements were performed using a HORIBA DeltaFlex-01-DD fluorescence lifetime system operated in time-correlated single counting mode. A delta laser diode (λ = 512 nm) was used for the excitation of thin film samples. Full width at half-maximum of the excitation source was 208 ps. PL emission was detected with a single-photon counting hybrid picosecond photon detector, and the obtained data were analyzed using EzTime and decay fit software.

Device Fabrication and Characterization. For the device fabrication, initially, the patterned indium tin oxide (ITO) substrates with resistivity ∼10 ohm-cm and transmittance 85% were cleaned with detergent followed by 20 min ultrasonification in deionized water, methanol, acetone, and isopropanol, sequentially. Subsequently, the ultraviolet−ozone treatment was carried out on cleaned ITO substrates for 20 min. Then, the ZnO solution was spin-coated on ITO substrates at 3500 rpm followed by annealing at 250 °C for 20 min. The active layer concentration and its donor−acceptor weight ratio are summarized in the Supporting Information. The spin coating of the active layer was performed in a nitrogen environment with different rotation speeds for different active layers to obtain films with thickness around 100 nm. Finally, 10 nm-thick molybdenum trioxide and 100 nm-thick silver layers were thermally evaporated through a shadow mask. The current density−voltage ($J-V$) measurements were performed using a Keithley 2400 source meter under AM 1.5G illumination. The active area for all the devices was defined as 4 mm^2 using a shadow aperture mask. EQE spectra were acquired using an incident photon to charge conversion efficiency setup (PVE300, Bentham Instruments) equipped with a standard silicon cell to calibrate the light source.

E_g Calculation. The E_g values were estimated from the EQE spectra of fully functional devices, which has its own advantages, such as being easily accessible and excluding influences of morphological effects. The EQE spectrum is not only correlated with the intrinsic

https://doi.org/10.1021/acsami.2c18199
ACS Appl. Mater. Interfaces XXXX, XXX, XXX−XXX

internal properties of absorbing materials and intermixing of D−A in blend, but also dependent on the device structure (thickness of active layer and optical properties of interlayers and electrodes) because the interference effects can slightly change the shape of the EQE spectrum.[52,67] In this study, we interpret the first derivative of EQE (d/dE(EQE)) as a distribution of SQ-type band gaps. From this distribution, the photovoltaic bandgap (E_g) was determined, and the respective analyses for all the devices are shown in Figure S1.

Voltage Loss Calculations. The voltage loss of the fabricated devices is mathematically expressed as the difference between the bandgap (E_g) and its open circuit voltage (V_{OC}).

$$\Delta V_{OC} = E_g/q - V_{OC} \tag{1}$$

Furthermore, when comparing V_{OC} with its radiative limit and thermodynamically SQ limit, it allows us to categorize the ΔV_{OC} into three different types.[21]

$$\Delta V_{OC} = (E_g/q - V_{OC,SQ}) + (V_{OC,SQ} - V_{OC,rad}) + (V_{OC,rad} - V_{OC}) \tag{2}$$

$$\Delta V_{OC} = \Delta V_{OC,SQ} + \Delta V_{OC,rad} + \Delta V_{OC,nrad} \tag{3}$$

where $\Delta V_{OC,SQ}$ is the thermodynamically inevitable loss limited by the detailed balance between absorbed and emitted photons in thermal equilibrium, $\Delta V_{OC,rad}$ is the radiative voltage loss caused by the absorption below the optical bandgap in actual devices, and $\Delta V_{OC,nrad}$ is the voltage loss due to the nonradiative recombination. $V_{OC,SQ}$ and $V_{OC,rad}$ are the fundamental unavoidable thermodynamic SQ limit and thermodynamic voltage limit without any nonradiative recombination for a particular E_g, irrespective of open circuit voltage, and it is expressed in terms of photon flux AM 1.5G and blackbody emission flux density as follows.

$$V_{OC,SQ} = \frac{k_B T}{q} \ln\left(\frac{\int_{E_g}^{\infty} \Phi_{AM1.5}(E).\,dE}{\int_{E_g}^{\infty} \Phi_{BB}(E).\,dE} + 1\right) \tag{4}$$

$$V_{OC,rad} = \frac{k_B T}{q} \ln\left(\frac{\int_{E_g}^{\infty} EQE(E)\,\Phi_{AM1.5}(E).\,dE}{\int_{E_g}^{\infty} EQE(E)\,\Phi_{BB}(E).\,dE} + 1\right) \tag{5}$$

Using EQE, E_g, and eqs 2−5, the different parts of V_{OC} losses were investigated for all the fabricated devices.

Urbach Energy. The Urbach energy of the photoactive layer can be estimated as by the exponential shape curve of the EQE spectra which is described by the following expression:[41]

$$EQE(E)\ \alpha\ \exp\left[\frac{E - E_g}{E_U}\right] \tag{6}$$

$$E_U = \left[\frac{d}{dE}(\ln(EQE))\right]^{-1} \tag{7}$$

where E_U is the tailing parameter related to the molecular disorder, which is generally referred as the Urbach energy.

■ ASSOCIATED CONTENT

Supporting Information

The Supporting Information is available free of charge at https://pubs.acs.org/doi/10.1021/acsami.2c18199.

List of materials used, energy level of the pristine donor and acceptor, active layer concentration, ratio, solvent, and additives, exciton lifetime and PL quenching of the pristine materials and photoactive layer, schematic of determination of E_g, and fitting of EQE spectra from exponential-shaped band-edges of the 13-active layer (PDF)

■ AUTHOR INFORMATION

Corresponding Author

Supravat Karak − *Organic and Hybrid Electronic Device Laboratory, Department of Energy Science and Engineering, Indian Institute of Technology Delhi, New Delhi 110016, India;* orcid.org/0000-0002-0650-8353; Email: supravat@iitd.ac.in

Authors

Rakesh Suthar − *Organic and Hybrid Electronic Device Laboratory, Department of Energy Science and Engineering, Indian Institute of Technology Delhi, New Delhi 110016, India;* orcid.org/0000-0002-3921-2639

Abhijith T − *Organic and Hybrid Electronic Device Laboratory, Department of Energy Science and Engineering, Indian Institute of Technology Delhi, New Delhi 110016, India*

Hemraj Dahiya − *Department of Physics, The LNM Institute of Information Technology, Jaipur, Rajasthan 302031, India;* orcid.org/0000-0002-1427-2758

Abhishek Kumar Singh − *Department of Electronics Engineering, Rajiv Gandhi Institute of Petroleum Technology, Amethi, Uttar Pradesh 229304, India*

Ganesh D Sharma − *Department of Physics, The LNM Institute of Information Technology, Jaipur, Rajasthan 302031, India*

Complete contact information is available at: https://pubs.acs.org/10.1021/acsami.2c18199

Author Contributions

R.S.: Conceptualization, investigation, software, data curation, and writing original draft. A.T.: Investigation, data curation, and writing − review & editing. H.D.: Investigation and formal analysis. A.K.S.: Investigation and formal analysis. G.D.S.: Supervision and writing − review & editing. S.K.: Supervision, conceptualization, and writing − review & editing.

Notes

The authors declare no competing financial interest.

■ ACKNOWLEDGMENTS

We would like to acknowledge Nanoscale Research Facility (NRF) and Central Research Facility (CRF) at Indian Institute of Technology (IIT) Delhi for providing the characterization facilities.

■ REFERENCES

(1) Heeger, A. J. 25th Anniversary Article: Bulk Heterojunction Solar Cells: Understanding the Mechanism of Operation. *Adv. Mater.* **2014**, *26*, 10−28.

(2) Lu, L.; Zheng, T.; Wu, Q.; Schneider, A. M.; Zhao, D.; Yu, L. Recent Advances in Bulk Heterojunction Polymer Solar Cells. *Chem. Rev.* **2015**, *115*, 12666−12731.

(3) Zhang, G.; Lin, F. R.; Qi, F.; Heumüller, T.; Distler, A.; Egelhaaf, H.-J.; Li, N.; Chow, P. C. Y.; Brabec, C. J.; Jen, A. K.-Y.; Yip, H.-L. Renewed Prospects for Organic Photovoltaics. *Chem. Rev.* **2022**, 14180.

(4) Yao, H.; Hou, J. Recent Advances in Single-Junction Organic Solar Cells. *Angew. Chem. Int. Ed.* **2022**, *61*, No. e202209021.

(5) Li, Y.; Xu, G.; Cui, C.; Li, Y. Flexible and Semitransparent Organic Solar Cells. *Adv. Energy Mater.* **2018**, *8*, No. 1701791.

(6) Di Carlo Rasi, D.; Janssen, R. A. J. Advances in Solution-Processed Multijunction Organic Solar Cells. *Adv. Mater.* **2019**, *31*, No. 1806499.

(7) Duan, L.; Hoex, B.; Uddin, A. Progress in Semitransparent Organic Solar Cells. *Sol. RRL* **2021**, *5*, No. 2100041.
(8) Riede, M.; Spoltore, D.; Leo, K. Organic Solar Cells-The Path to Commercial Success. *Adv. Energy Mater.* **2021**, *11*, No. 2002653.
(9) Zhang, G.; Zhao, J.; Chow, P. C. Y.; Jiang, K.; Zhang, J.; Zhu, Z.; Zhang, J.; Huang, F.; Yan, H. Nonfullerene Acceptor Molecules for Bulk Heterojunction Organic Solar Cells. *Chem. Rev.* **2018**, *118*, 3447−3507.
(10) Ma, L.; Zhang, S.; Wang, J.; Xu, Y.; Hou, J. Recent Advances in Non-Fullerene Organic Solar Cells: From Lab to Fab. *Chem. Commun.* **2020**, *56*, 14337−14352.
(11) Duan, L.; Uddin, A. Progress in Stability of Organic Solar Cells. *Adv. Sci.* **2020**, *7*, No. 1903259.
(12) Cui, Y.; Xu, Y.; Yao, H.; Bi, P.; Hong, L.; Zhang, J.; Zu, Y.; Zhang, T.; Qin, J.; Ren, J.; Chen, Z.; He, C.; Hao, X.; Wei, Z.; Hou, J. Single-Junction Organic Photovoltaic Cell with 19% Efficiency. *Adv. Mater.* **2021**, *33*, No. 2102420.
(13) He, C.; Pan, Y.; Ouyang, Y.; Shen, Q.; Gao, Y.; Yan, K.; Fang, J.; Chen, Y.; Ma, C.-Q.; Min, J.; Zhang, C.; Zuo, L.; Chen, H. Manipulating the D:A Interfacial Energetics and Intermolecular Packing for 19.2% Efficiency Organic Photovoltaics. *Energy Environ. Sci.* **2022**, *15*, 2537−2544.
(14) Sun, R.; Wu, Y.; Yang, X.; Gao, Y.; Chen, Z.; Li, K.; Qiao, J.; Wang, T.; Guo, J.; Liu, C.; Hao, X.; Zhu, H.; Min, J. Single-Junction Organic Solar Cells with 19.17% Efficiency Enabled by Introducing One Asymmetric Guest Acceptor. *Adv. Mater.* **2022**, *34*, No. 2110147.
(15) Gao, W.; Qi, F.; Peng, Z.; Lin, F. R.; Jiang, K.; Zhong, C.; Kaminsky, W.; Guan, Z.; Lee, C.-S.; Marks, T. J.; Ade, H.; Jen, A. K.-Y. Achieving 19% Power Conversion Efficiency in Planar-Mixed Heterojunction Organic Solar Cells Using a Pseudosymmetric Electron Acceptor. *Adv. Mater.* **2022**, *34*, No. 2202089.
(16) Zhu, L.; Zhang, M.; Xu, J.; Li, C.; Yan, J.; Zhou, G.; Zhong, W.; Hao, T.; Song, J.; Xue, X.; Zhou, Z.; Zeng, R.; Zhu, H.; Chen, C. C.; MacKenzie, R. C. I.; Zou, Y.; Nelson, J.; Zhang, Y.; Sun, Y.; Liu, F. Single-Junction Organic Solar Cells with over 19% Efficiency Enabled by a Refined Double-Fibril Network Morphology. *Nat. Mater.* **2022**, *21*, 656−663.
(17) Dahiya, H.; Suthar, R.; Khandelwal, K.; Karak, S.; Sharma, G. D. Recent Advances in Organic and Inorganic Hole and Electron Transport Layers for Organic Solar Cells: Basic Concept and Device Performance. *ACS Appl. Electron. Mater.* **2022**, *4*, 5119−5143.
(18) Suthar, R.; Dahiya, H.; Karak, S.; Sharma, G. D. Ternary Organic Solar Cells: Recent Insight on Structure−Processing−Property−Performance Relationships. *Energy Technol.* **2022**, No. 2201176.
(19) Karuthedath, S.; Gorenflot, J.; Firdaus, Y.; Chaturvedi, N.; De Castro, C. S. P.; Harrison, G. T.; Khan, J. I.; Markina, A.; Balawi, A. H.; Peña, T. A. D.; Lopatin, S.; Anjum, D. H.; Beaujuge, P. M.; De Wolf, S.; McCulloch, I.; Anthopoulos, T. D.; Baran, D.; Andrienko, D.; Laquai, F. Intrinsic Efficiency Limits in Low-Bandgap Non-Fullerene Acceptor Organic Solar Cells. *Nat. Mater.* **2021**, *20*, 378−384.
(20) Markina, A.; Lin, K. H.; Liu, W.; Poelking, C.; Firdaus, Y.; Villalva, D. R.; Khan, J. I.; Paleti, S. H. K.; Harrison, G. T.; Gorenflot, J.; Zhang, W.; De Wolf, S.; McCulloch, I.; Anthopoulos, T. D.; Baran, D.; Laquai, F.; Andrienko, D. Chemical Design Rules for Non-Fullerene Acceptors in Organic Solar Cells. *Adv. Energy Mater.* **2021**, *11*, No. 2102363.
(21) Hou, J.; Inganas, O.; Friend, R. H.; Gao, F. Organic Solar Cells Based on Non-Fullerene Acceptors. *Nat. Mater.* **2018**, *17*, 119−128.
(22) Vandewal, K.; Tvingstedt, K.; Gadisa, A.; Inganäs, O.; Manca, J. V. On the Origin of the Open-Circuit Voltage of Polymer-Fullerene Solar Cells. *Nat. Mater.* **2009**, *8*, 904−909.
(23) Wang, J.; Yao, H.; Xu, Y.; Ma, L.; Hou, J. Recent Progress in Reducing Voltage Loss in Organic Photovoltaic Cells. *Mater. Chem. Front.* **2021**, *5*, 709−722.
(24) Polman, A.; Knight, M.; Garnett, E. C.; Ehrler, B.; Sinke, W. C. Photovoltaic Materials: Present Efficiencies and Future Challenges. *Science* **2016**, *352*, No. aad4424.
(25) Liu, Z.; Krückemeier, L.; Krogmeier, B.; Klingebiel, B.; Márquez, J. A.; Levcenko, S.; Öz, S.; Mathur, S.; Rau, U.; Unold, T.; Kirchartz, T. Open-Circuit Voltages Exceeding 1.26 V in Planar Methylammonium Lead Iodide Perovskite Solar Cells. *ACS Energy Lett.* **2019**, *4*, 110−117.
(26) Eisner, F. D.; Azzouzi, M.; Fei, Z.; Hou, X.; Anthopoulos, T. D.; Dennis, T. J. S.; Heeney, M.; Nelson, J. Hybridization of Local Exciton and Charge-Transfer States Reduces Nonradiative Voltage Losses in Organic Solar Cells. *J. Am. Chem. Soc.* **2019**, *141*, 6362−6374.
(27) Sharma, R.; Jain, N.; Lee, H.; Kabra, D.; Yoo, S. Comprehensive and Comparative Analysis of Photoinduced Charge Generation, Recombination Kinetics, and Energy Losses in Fullerene and Nonfullerene Acceptor-Based Organic Solar Cells. *ACS Appl. Mater. Interfaces* **2020**, *12*, 45083−45091.
(28) Dong, Y.; Cha, H.; Bristow, H. L.; Lee, J.; Kumar, A.; Tuladhar, P. S.; McCulloch, I.; Bakulin, A. A.; Durrant, J. R. Correlating Charge-Transfer State Lifetimes with Material Energetics in Polymer:Non-Fullerene Acceptor Organic Solar Cells. *J. Am. Chem. Soc.* **2021**, *143*, 7599−7603.
(29) Scharber, M. C.; Mühlbacher, D.; Koppe, M.; Denk, P.; Waldauf, C.; Heeger, A. J.; Brabec, C. J. Design Rules for Donors in Bulk-Heterojunction Solar Cells - Towards 10% Energy-Conversion Efficiency. *Adv. Mater.* **2006**, *18*, 789−794.
(30) Clarke, T. M.; Durrant, J. R. Charge Photogeneration in Organic Solar Cells. *Chem. Rev.* **2010**, *110*, 6736−6767.
(31) Dennler, G.; Scharber, M. C.; Brabec, C. J. Polymer-Fullerene Bulk-Heterojunction Solar Cells. *Adv. Mater.* **2009**, *21*, 1323−1338.
(32) Veldman, D.; Meskers, S. C. J.; Janssen, R. A. J. The Energy of Charge-Transfer States in Electron Donor-Acceptor Blends: Insight into the Energy Losses in Organic Solar Cells. *Adv. Funct. Mater.* **2009**, *19*, 1939−1948.
(33) Zheng, Z.; Yao, H.; Ye, L.; Xu, Y.; Zhang, S.; Hou, J. PBDB-T and Its Derivatives: A Family of Polymer Donors Enables over 17% Efficiency in Organic Photovoltaics. *Mater. Today* **2020**, *35*, 115−130.
(34) Chen, X.-K.; Qian, D.; Wang, Y.; Kirchartz, T.; Tress, W.; Yao, H.; Yuan, J.; Hülsbeck, M.; Zhang, M.; Zou, Y.; Sun, Y.; Li, Y.; Hou, J.; Inganäs, O.; Coropceanu, V.; Bredas, J.-L.; Gao, F. A Unified Description of Non-Radiative Voltage Losses in Organic Solar Cells. *Nat. Energy* **2021**, *6*, 799−806.
(35) Xie, Y.; Wang, W.; Huang, W.; Lin, F.; Li, T.; Liu, S.; Zhan, X.; Liang, Y.; Gao, C.; Wu, H.; Cao, Y. Assessing the Energy Offset at the Electron Donor/Acceptor Interface in Organic Solar Cells through Radiative Efficiency Measurements. *Energy Environ. Sci.* **2019**, *12*, 3556−3566.
(36) Gasparini, N.; Camargo, F. V. A.; Frühwald, S.; Nagahara, T.; Classen, A.; Roland, S.; Wadsworth, A.; Gregoriou, V. G.; Chochos, C. L.; Neher, D.; Salvador, M.; Baran, D.; McCulloch, I.; Görling, A.; Lüer, L.; Cerullo, G.; Brabec, C. J. Adjusting the Energy of Interfacial States in Organic Photovoltaics for Maximum Efficiency. *Nat. Commun.* **2021**, *12*, 1772.
(37) Qian, D.; Zheng, Z.; Yao, H.; Tress, W.; Hopper, T. R.; Chen, S.; Li, S.; Liu, J.; Chen, S.; Zhang, J.; Liu, X.-K.; Gao, B.; Ouyang, L.; Jin, Y.; Pozina, G.; Buyanova, I. A.; Chen, W. M.; Inganäs, O.; Coropceanu, V.; Bredas, J.-L.; Yan, H.; Hou, J.; Zhang, F.; Bakulin, A. A.; Gao, F. Design Rules for Minimizing Voltage Losses in High-Efficiency Organic Solar Cells. *Nat. Mater.* **2018**, *17*, 703−709.
(38) Kuik, M.; Koster, L. J. A.; Wetzelaer, G. A. H.; Blom, P. W. M. Trap-Assisted Recombination in Disordered Organic Semiconductors. *Phys. Rev. Lett.* **2011**, *107*, No. 256805.
(39) Yang, Y.; Chen, W.; Dou, L.; Chang, W.-H.; Duan, H.-S.; Bob, B.; Li, G.; Yang, Y. High-Performance Multiple-Donor Bulk Heterojunction Solar Cells. *Nat. Photonics* **2015**, *9*, 190−198.
(40) Kirchartz, T.; Pieters, B. E.; Kirkpatrick, J.; Rau, U.; Nelson, J. Recombination via Tail States in Polythiophene:Fullerene Solar Cells. *Phys. Rev. B Condens. Matter Mater. Phys.* **2011**, *83*, No. 115209.
(41) Yuan, J.; Zhang, C.; Qiu, B.; Liu, W.; So, S. K.; Mainville, M.; Leclerc, M.; Shoaee, S.; Neher, D.; Zou, Y. Effects of Energetic

https://doi.org/10.1021/acsami.2c18199
ACS Appl. Mater. Interfaces XXXX, XXX, XXX−XXX

Disorder in Bulk Heterojunction Organic Solar Cells. *Energy Environ. Sci.* **2022**, *15*, 2806−2818.
(42) Classen, A.; Chochos, C. L.; Lüer, L.; Gregoriou, V. G.; Wortmann, J.; Osvet, A.; Forberich, K.; McCulloch, I.; Heumüller, T.; Brabec, C. J. The Role of Exciton Lifetime for Charge Generation in Organic Solar Cells at Negligible Energy-Level Offsets. *Nat. Energy* **2020**, *5*, 711−719.
(43) Riley, D. B.; Meredith, P.; Armin, A.; Sandberg, O. J. Role of Exciton Diffusion and Lifetime in Organic Solar Cells with a Low Energy Offset. *J. Phys. Chem. Lett.* **2022**, *13*, 4402−4409.
(44) Sandberg, O. J.; Armin, A. Energetics and Kinetics Requirements for Organic Solar Cells to Break the 20% Power Conversion Efficiency Barrier. *J. Phys. Chem. C* **2021**, *125*, 15590−15598.
(45) Liu, H.; Li, M.; Wu, H.; Wang, J.; Ma, Z.; Tang, Z. Improving Quantum Efficiency in Organic Solar Cells with a Small Energetic Driving Force. *J. Mater. Chem. A* **2021**, *9*, 19770−19777.
(46) Yang, C.; Zhang, J.; Liang, N.; Yao, H.; Wei, Z.; He, C.; Yuan, X.; Hou, J. Effects of Energy-Level Offset between a Donor and Acceptor on the Photovoltaic Performance of Non-Fullerene Organic Solar Cells. *J. Mater. Chem. A* **2019**, *7*, 18889−18897.
(47) Liu, S.; Yuan, J.; Deng, W.; Luo, M.; Xie, Y.; Liang, Q.; Zou, Y.; He, Z.; Wu, H.; Cao, Y. High-Efficiency Organic Solar Cells with Low Non-Radiative Recombination Loss and Low Energetic Disorder. *Nat. Photonics* **2020**, *14*, 300−305.
(48) Guo, Q.; Liu, Y.; Liu, M.; Zhang, H.; Qian, X.; Yang, J.; Wang, J.; Xue, W.; Zhao, Q.; Xu, X.; Ma, W.; Tang, Z.; Li, Y.; Bo, Z. Enhancing the Performance of Organic Solar Cells by Prolonging the Lifetime of Photogenerated Excitons. *Adv. Mater.* **2020**, *32*, No. 2003164.
(49) Riley, D. B.; Sandberg, O. J.; Li, W.; Meredith, P.; Armin, A. Quasi-Steady-State Measurement of Exciton Diffusion Lengths in Organic Semiconductors. *Phys. Rev. Appl.* **2022**, *17*, No. 024076.
(50) Yao, J.; Kirchartz, T.; Vezie, M. S.; Faist, M. A.; Gong, W.; He, Z.; Wu, H.; Troughton, J.; Watson, T.; Bryant, D.; Nelson, J. Quantifying Losses in Open-Circuit Voltage in Solution-Processable Solar Cells. *Phys. Rev. Appl.* **2015**, *4*, No. 014020.
(51) Wang, Y.; Qian, D.; Cui, Y.; Zhang, H.; Hou, J.; Vandewal, K.; Kirchartz, T.; Gao, F. Optical Gaps of Organic Solar Cells as a Reference for Comparing Voltage Losses. *Adv. Energy Mater.* **2018**, *8*, No. 1801352.
(52) Rau, U.; Blank, B.; Müller, T. C. M.; Kirchartz, T. Efficiency Potential of Photovoltaic Materials and Devices Unveiled by Detailed-Balance Analysis. *Phys. Rev. Appl.* **2017**, *7*, No. 044016.
(53) Vandewal, K.; Benduhn, J.; Nikolis, V. C. How to Determine Optical Gaps and Voltage Losses in Organic Photovoltaic Materials. *Sustain. Energy Fuels* **2018**, *2*, 538−544.
(54) Ji, Y.; Xu, L.; Hao, X.; Gao, K. Energy Loss in Organic Solar Cells: Mechanisms, Strategies, and Prospects. *Sol. RRL* **2020**, *4*, No. 2000130.
(55) Yoshikawa, K.; Kawasaki, H.; Yoshida, W.; Irie, T.; Konishi, K.; Nakano, K.; Uto, T.; Adachi, D.; Kanematsu, M.; Uzu, H.; Yamamoto, K. Silicon Heterojunction Solar Cell with Interdigitated Back Contacts for a Photoconversion Efficiency over 26%. *Nat. Energy* **2017**, *2*, 17032.
(56) Miller, O. D.; Yablonovitch, E.; Kurtz, S. R. Strong Internal and External Luminescence as Solar Cells Approach the Shockley−Queisser Limit. *IEEE J. Photovoltaics* **2012**, *2*, 303−311.
(57) Gillett, A. J.; Privitera, A.; Dilmurat, R.; Karki, A.; Qian, D.; Pershin, A.; Londi, G.; Myers, W. K.; Lee, J.; Yuan, J.; Ko, S.-J.; Riede, M. K.; Gao, F.; Bazan, G. C.; Rao, A.; Nguyen, T.-Q.; Beljonne, D.; Friend, R. H. The Role of Charge Recombination to Triplet Excitons in Organic Solar Cells. *Nature* **2021**, *597*, 666−671.
(58) Wu, J.; Lee, J.; Chin, Y. C.; Yao, H.; Cha, H.; Luke, J.; Hou, J.; Kim, J. S.; Durrant, J. R. Exceptionally Low Charge Trapping Enables Highly Efficient Organic Bulk Heterojunction Solar Cells. *Energy Environ. Sci.* **2020**, *13*, 2422−2430.
(59) Falsini, N.; Roini, G.; Ristori, A.; Calisi, N.; Biccari, F.; Vinattieri, A. Analysis of the Urbach Tail in Cesium Lead Halide Perovskites. *J. Appl. Phys.* **2022**, *131*, No. 010902.
(60) Hu, W.; He, X.; Fang, Z.; Lian, W.; Shang, Y.; Li, X.; Zhou, W.; Zhang, M.; Chen, T.; Lu, Y.; Zhang, L.; Ding, L.; Yang, S. Bulk Heterojunction Gifts Bismuth-Based Lead-Free Perovskite Solar Cells with Record Efficiency. *Nano Energy* **2020**, *68*, No. 104362.
(61) Beaudoin, M.; DeVries, A. J. G.; Johnson, S. R.; Laman, H.; Tiedje, T. Optical Absorption Edge of Semi-Insulating GaAs and InP at High Temperatures. *Appl. Phys. Lett.* **1997**, *70*, 3540−3542.
(62) Göhler, C.; Deibel, C. The Role of Dynamic and Static Disorder for Charge-Transfer States in Organic Bulk Heterojunction Solar Cells. *ACS Energy Lett.* **2022**, *7*, 2156−2164.
(63) Zhang, C.; Mahadevan, S.; Yuan, J.; Ho, J. K. W.; Gao, Y.; Liu, W.; Zhong, H.; Yan, H.; Zou, Y.; Tsang, S.-W.; So, S. K. Unraveling Urbach Tail Effects in High-Performance Organic Photovoltaics: Dynamic vs Static Disorder. *ACS Energy Lett.* **2022**, *7*, 1971−1979.
(64) Ugur, E.; Ledinský, M.; Allen, T. G.; Holovský, J.; Vlk, A.; De Wolf, S. Life on the Urbach Edge. *J. Phys. Chem. Lett.* **2022**, *13*, 7702−7711.
(65) Bisquert, J. Unique Curve for the Radiative Photovoltage Deficit Caused by the Urbach Tail. *J. Phys. Chem. Lett.* **2021**, *12*, 7840−7845.
(66) Panhans, M.; Hutsch; Sebastian; Benduhn, J.; Schellhammer, K. S.; Nikolis, V. C.; Vangerven, T.; Vandewal, K.; Ortmann, F. Molecular Vibrations Reduce the Maximum Achievable Photovoltage in Organic Solar Cells. *Nat. Commun.* **2020**, *11*, 1488.
(67) Bertrandie, J.; Han, J.; De Castro, C. S. P.; Yengel, E.; Gorenflot, J.; Anthopoulos, T.; Laquai, F.; Sharma, A.; Baran, D. The Energy Level Conundrum of Organic Semiconductors in Solar Cells. *Adv. Mater.* **2022**, *34*, No. 2202575.

https://doi.org/10.1021/acsami.2c18199
ACS Appl. Mater. Interfaces XXXX, XXX, XXX−XXX